

Journal of Geophysical Research Solid Earth

Volume 119 Issue 12 December 2014

JGREA2(12) 8577–9236 (2014)

ISSN 2169-9313 (print); ISSN 2169-9356 (Online)

The online article is the official version and may contain additional content not available in this print issue. To access the full article, including multimedia, enhanced figures, supporting information, and other nonprinted content, go to <http://wileyonlinelibrary.com/journal/jgrb>.

Geomagnetism and Paleomagnetism/Marine Geology and Geophysics

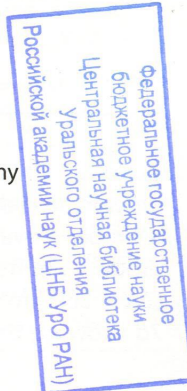
- 8577** Zsuzsanna Tóth, Volkhard Spiess, José M. Mogollón, and Jørn Bo Jensen
Estimating the free gas content in Baltic Sea sediments using compressional wave velocity from marine seismic data (doi 10.1002/2014JB010989)
- 8594** Benjamin J. Phrampus, Matthew J. Hornbach, Carolyn D. Ruppel, and Patrick E. Hart
Widespread gas hydrate instability on the upper U.S. Beaufort margin (doi 10.1002/2014JB011290)
- 8610** Tabea Altenbernd, Wilfried Jokat, Ingo Heyde, and Volkmar Damm
A crustal model for northern Melville Bay, Baffin Bay (doi 10.1002/2014JB011559)
- 8633** Evgeniy V. Kulakov, Aleksey V. Smirnov, and Jimmy F. Diehl
Paleomagnetism of the ~1.1Ga Coldwell Complex (Ontario, Canada): Implications for Proterozoic geomagnetic field morphology and plate velocities (doi 10.1002/2014JB011463)
- 8655** Kaushalendra M. Bhatt
Microseisms and its impact on the marine-controlled source electromagnetic signal (doi 10.1002/2014JB011024)

Chemistry and Physics of Minerals and Rocks/Volcanology

- 8667** Társilo Girona, Fidel Costa, Chris Newhall, and Benoit Taisne
On depressurization of volcanic magma reservoirs by passive degassing (doi 10.1002/2014JB011368)
- 8688** Jean Vandemeulebrouck, Robert A. Sohn, Maxwell L. Rudolph, Shaul Hurwitz, Michael Manga, Malcolm J. S. Johnston, S. Adam Soule, Darcy McPhee, Jonathan M. G. Glen, Leif Karlstrom, and Fred Murphy
Eruptions at Lone Star geyser, Yellowstone National Park, USA: 2. Constraints on subsurface dynamics (doi 10.1002/2014JB011526)
- 8708** Simon Virgo, Steffen Abe, and Janos L. Urai
The evolution of crack seal vein and fracture networks in an evolving stress field: Insights from Discrete Element Models of fracture sealing (doi 10.1002/2014JB011520)
- 8728** Anne M. H. Pluymakers, Jon E. Samuelson, André R. Niemeijer, and Christopher J. Spiers
Effects of temperature and CO₂ on the frictional behavior of simulated anhydrite fault rock (doi 10.1002/2014JB011575)
- 8748** C. E. Neuzil and A. M. Provost
Ice sheet load cycling and fluid underpressures in the Eastern Michigan Basin, Ontario, Canada (doi 10.1002/2014JB011643)
- 8770** N. M. Beeler, Terry Tullis, Jenni Junger, Brian Kilgore, and David Goldsby
Laboratory constraints on models of earthquake recurrence (doi 10.1002/2014JB011184)
- 8792** Fabian B. Wadsworth, Jérémie Vasseur, Felix W. von Aulock, Kai-Uwe Hess, Bettina Scheu, Yan Lavallée, and Donald B. Dingwell
Nonisothermal viscous sintering of volcanic ash (doi 10.1002/2014JB011453)
- 8805** Jacopo Selva, Antonio Costa, Laura Sandri, Giovanni Macedonio, and Warner Marzocchi
Probabilistic short-term volcanic hazard in phases of unrest: A case study for tephra fallout (doi 10.1002/2014JB011252)

Seismology

- 8827** Taka'aki Taira, Roland Bürgmann, Robert M. Nadeau, and Douglas S. Dreger
Variability of fault slip behavior along the San Andreas Fault in the San Juan Bautista Region (doi 10.1002/2014JB011427)
- 8845** Yun Wang and Carl Tape
Seismic velocity structure and anisotropy of the Alaska subduction zone based on surface wave tomography (doi 10.1002/2014JB011438)
- 8866** K. Michael Cleveland, Charles J. Ammon, and Thorne Lay
Large earthquake processes in the northern Vanuatu subduction zone (doi 10.1002/2014JB011289)
- 8884** A. Hofstetter and C. Dorbath
Teleseismic traveltimes residuals across the Dead Sea basin (doi 10.1002/2014JB011357)
- 8900** O. Lengliné, L. Lamourette, L. Vivin, N. Cuenot, and J. Schmittbuhl
Fluid-induced earthquakes with variable stress drop (doi 10.1002/2014JB011282)
- 8914** Mairéad Nic Bhloscaidh, John McCloskey, and Christopher J. Bean
Response of the San Jacinto Fault Zone to static stress changes from the 1992 Landers earthquake (doi 10.1002/2014JB011164)



0148-0227JB-119-12

- 8936** *Quan Gan and Derek Elsworth*
Thermal drawdown and late-stage seismic-slip fault reactivation in enhanced geothermal reservoirs
(doi 10.1002/2014JB011323)
- 8950** *Lisa Linville, Kristine Pankow, Debi Kilb, and Aaron Velasco*
Exploring remote earthquake triggering potential across EarthScopes' Transportable Array through frequency domain array visualization (doi 10.1002/2014JB011529)
- 8964** *Tatsunori Ikeda and Takeshi Tsuji*
Azimuthal anisotropy of Rayleigh waves in the crust in southern Tohoku area, Japan (doi 10.1002/2014JB011567)
- 8976** *Hongfeng Yang, Zefeng Li, Zhigang Peng, Yehuda Ben-Zion, and Frank Vernon*
Low-velocity zones along the San Jacinto Fault, Southern California, from body waves recorded in dense linear arrays
(doi 10.1002/2014JB011548)
- 8991** *S. J. Bourne, S. J. Oates, J. van Elk, and D. Doornhof*
A seismological model for earthquakes induced by fluid extraction from a subsurface reservoir
(doi 10.1002/2014JB011663)
- 9016** *Keisuke Yoshida, Akira Hasegawa, Tomomi Okada, and Takeshi Iinuma*
Changes in the stress field after the 2008 M7.2 Iwate-Miyagi Nairiku earthquake in northeastern Japan
(doi 10.1002/2014JB011291)
- Geodesy and Gravity/Tectonophysics**
- 9031** *Changyi Xu, Wenke Sun, and B. Fong Chao*
Formulation of coseismic changes in Earth rotation and low-degree gravity field based on the spherical Earth dislocation theory (doi 10.1002/2014JB011328)
- 9042** *Zoltán Erdős, Ritske S. Huismans, Peter van der Beek, and Cedric Thieulot*
Extensional inheritance and surface processes as controlling factors of mountain belt structure
(doi 10.1002/2014JB011408)
- 9062** *B. M. Carpenter, M. M. Scuderi, C. Collettini, and C. Marone*
Frictional heterogeneities on carbonate-bearing normal faults: Insights from the Monte Maggio Fault, Italy
(doi 10.1002/2014JB011337)
- 9077** *Luca Smeraglia, Fabio Trippetta, Eugenio Carminati, and Silvio Mollo*
Tectonic control on the petrophysical properties of foredeep sandstone in the Central Apennines, Italy
(doi 10.1002/2014JB011221)
- 9095** *Laurent Métivier, Xavier Collilieux, Daphné Lercier, Zuheir Altamimi, and François Beauducel*
Global coseismic deformations, GNSS time series analysis, and earthquake scaling laws (doi 10.1002/2014JB011280)
- 9110** *Timothy J. Craig and Eric Calais*
Strain accumulation in the New Madrid and Wabash Valley seismic zones from 14 years of continuous GPS observation
(doi 10.1002/2014JB011498)
- 9130** *C. Jaupart, J.-C. Mareschal, H. Bouquerel, and C. Phaneuf*
The building and stabilization of an Archean Craton in the Superior Province, Canada, from a heat flow perspective
(doi 10.1002/2014JB011018)
- 9156** *David Eriksson, D. S. MacMillan, and John M. Gipson*
Tropospheric delay ray tracing applied in VLBI analysis (doi 10.1002/2014JB011552)
- 9171** *Yngve Kristoffersen, Coen Hofstede, Anja Diez, Richard Blenkner, Astrid Lambrecht, Christoph Mayer, and Olaf Eisen*
Reassembling Gondwana: A new high quality constraint from vibroseis exploration of the sub-ice shelf geology of the East Antarctic continental margin (doi 10.1002/2014JB011479)
- 9183** *Gal Hartman, Tina M. Niemi, Gideon Tibor, Zvi Ben-Avraham, Abdallah Al-Zoubi, Yizhaq Makovsky, Emad Akawwi, Abdel-Rahman Abueladas, and Rami Al-Ruzouq*
Quaternary tectonic evolution of the Northern Gulf of Elat/Aqaba along the Dead Sea Transform (doi 10.1002/2013JB010879)
- 9206** *Gaël Choblet, Laurent Husson, and Thomas Bodin*
Probabilistic surface reconstruction of coastal sea level rise during the twentieth century (doi 10.1002/2014JB011639)

Cover. In Erdos et al. [DOI: 10.1002/2014JB011408], image shows model M5 including simple sedimentation and erosion models. Sedimentation is accounted for with the same algorithm as in model M4. Erosion is modeled using a simple elevation-dependent algorithm. We have scaled the erosion rate so that a 4 km high topography would erode 1 km in 2 Myr. Presenting the same model properties as in the reference model (Figure 2) after (a) 30 Myr ($\Delta x = 200$ km) contraction and (d) 40 Myr ($\Delta x = 300$ km) contraction. (b) and (c) are zoomed extracts from Figure 7d showing the small-scale deformation patterns in the foreland fold-and-thrust belts. See pp. 9042-9061.